



Wafer-Scale Fabrication of High-Performance n-Type Polymer Monolayer Transistors Using a Multi-Level Self-Assembly Strategy

Ze-Fan Yao, Yu-Qing Zheng, Qi-Yi Li, Ting Lei,* Song Zhang, Lin Zou, Han-Yu Liu, Jin-Hu Dou, Yang Lu, Jie-Yu Wang, Xiaodan Gu, and Jian Pei*

Wafer-scale fabrication of high-performance uniform organic electronic materials is of great challenge and has rarely been realized before. Previous large-scale fabrication methods always lead to different layer thickness and thereby poor film and device uniformity. Herein, the first demonstration of 4 in. wafer-scale, uniform, and high-performance n-type polymer monolayer films is reported, enabled by controlling the multi-level self-assembly process of conjugated polymers in solution. Since the self-assembly process happened in solution, the uniform 2D polymer monolayers can be facily deposited on various substrates, and theoretically without size limitations. Polymer monolayer transistors exhibit high electron mobilities of up to $1.88 \text{ cm}^2 \text{ V}^{-1} \text{ s}^{-1}$, which is among the highest in n-type monolayer organic transistors. This method allows to easily fabricate n-type conjugated polymers with wafer-scale, high uniformity, low contact resistance, and excellent transistor performance (better than the traditional spin-coating method). This work provides an effective strategy to prepare large-scale and uniform 2D polymer monolayers, which could enable the application of conjugated polymers for wafer-scale sophisticated electronics.

unique physical and chemical properties, such as effective gate-controls, ultrahigh charge carrier mobilities,^[4] and quantum Hall features.^[5,6] Recently, 2D monolayers of conjugated molecules have been studied using solution processing or vacuum evaporation method.^[7–13] Compared to their thick films counterpart, ultrathin films exhibited some unique properties, such as uniform microstructure,^[3,14,15] constant carrier density,^[3] and high sensitivity as sensors.^[9,16] Like most 2D inorganic materials, fabrication of 2D organic materials is also of great challenges due to their weak van der Waals forces and variable lattice constants.^[3,17,18]

Many efforts have been devoted to the large-scale fabrication of the organic thin films,^[14,19–23] but only a few works realized 2D organic monolayers. Organic monolayers can avoid the film thickness variations and usually show less contact resistances.^[11,19] For example, He et al.

2D materials with atomic or molecular level thickness have attracted increasing interests due to their broad applications in optoelectronic devices, bio/chemical sensors, catalysis, and energy storage, etc.^[1–3] Their ultrathin body endows them with

demonstrated high hole mobilities and efficient charge injection in the monolayers of 2,7-dioctyl[1]benzothieno[3,2-b][1]benzothiophene (C8-BTBT).^[11] Li et al. demonstrated a polymer monolayer field-effect transistor (FET) exhibiting a high hole

Z.-F. Yao, Q.-Y. Li, H.-Y. Liu, Dr. J.-H. Dou, Y. Lu, Prof. J.-Y. Wang, Prof. J. Pei
Beijing National Laboratory for Molecular Sciences (BNLMS)
Key Laboratory of Bioorganic Chemistry
and Molecular Engineering of Ministry of Education
Key Laboratory of Polymer Chemistry
and Physics of Ministry of Education
Center of Soft Matter Science and Engineering
College of Chemistry and Molecular Engineering
Peking University
Beijing 100871, China
E-mail: jianpei@pku.edu.cn
Dr. Y.-Q. Zheng
Department of Chemical Engineering
Stanford University
Stanford, CA 94305, USA

Prof. T. Lei
Department of Materials Science and Engineering
College of Engineering
Peking University
Beijing 100871, China
E-mail: tinglei@pku.edu.cn
S. Zhang, Prof. X. Gu
School of Polymer Science and Engineering
The University of Southern Mississippi
Hattiesburg, MS 39406, USA
Dr. L. Zou
Institute of Nuclear Physics and Chemistry
China Academy of Engineering Physics
Mianyang 621900, China

The ORCID identification number(s) for the author(s) of this article can be found under <https://doi.org/10.1002/adma.201806747>.

DOI: 10.1002/adma.201806747

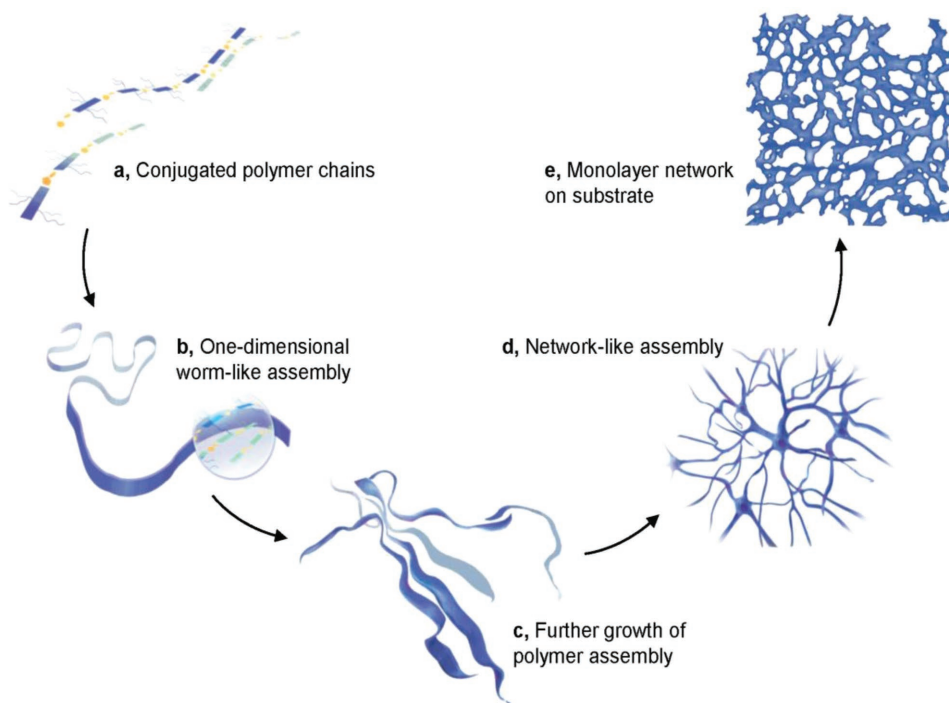


Figure 1. Proposed multi-level self-assembly process of a conjugated polymer. a) π - π stacking of the conjugated polymer backbones. b) 1D worm-like assemblies in solution. c) Further growth of polymer assemblies to larger aggregates. d) Proposed network-like assemblies in solution. e) Polymer monolayer networks deposited on a substrate.

mobility of $3 \text{ cm}^2 \text{ V}^{-1} \text{ s}^{-1}$.^[7] Shi et al. demonstrated a centimeter-scale n-type monolayer small-molecule crystal with a high electron mobility of $1.24 \text{ cm}^2 \text{ V}^{-1} \text{ s}^{-1}$.^[12] However, to our knowledge, high-performance n-type polymer monolayer FETs have not been realized, largely due to the limited numbers of n-type polymer materials and the air sensitivity of most n-type polymers. Compared to the p-type polymers, current state of the art n-type polymer monolayer FETs showed about 1–2 order lower mobilities (0.002 – $0.14 \text{ cm}^2 \text{ V}^{-1} \text{ s}^{-1}$).^[8–10,24] Moreover, wafer-scale fabrication of either p-type or n-type polymer monolayers is also challenging,^[9] because, in previous works, necessary film transfer process, unavoidable crystalline boundaries, or different layer thicknesses of 2D organic materials limited their uniformity for large-scale electronic devices.^[10,14,19,21]

Here, we report a new approach to obtain wafer-scale, uniform 2D polymer monolayer films by controlling the multi-level self-assembly process of an n-type conjugated polymer (**Figure 1**). We found that the formation and uniformity of the polymer monolayer are fully controlled by the polymer concentration and solvent properties. Moreover, such wafer-scale and uniform 2D monolayer can be deposited on different types of substrates with a wide fabrication condition window. Thin-film transistors (TFTs) based on the polymer monolayer networks exhibited air-stable n-type performance with high electron mobilities up to $1.88 \text{ cm}^2 \text{ V}^{-1} \text{ s}^{-1}$, comparable or even better than that of the conventional spin-coated thicker films. In addition, the 2D monolayer provides lower contact resistances due to less vertical charge transport distance. Based on multiple characterizations, we propose that this substrate-independent, uniform monolayer deposition strategy can be largely explained

by the controlled multi-level self-assembly process, where the polymer can form certain 2D-like networks in the solution state (**Figure 1**).

One of the great challenges in the scalable fabrication of conjugated polymer electronics is the uniformity requirement. It is difficult to produce large-scale and uniform thin films of conjugated polymers with uniform microstructure and device performance due to their complicated and changeable chain entanglement during the film-formation process.^[25] Because of the strong molecular interactions between conjugated backbones, they usually aggregate in solution.^[7,26,27] We propose that this feature might facilitate a multi-level self-assembly process, and finally lead to a large-scale, uniform, and ordered packed 2D polymer film. Diagram in **Figure 1** shows the growth process of conjugated polymer from 1D worm-like assemblies to 2D monolayer networks. As conjugated polymers assembling via strong π - π interaction (**Figure 1a**), 1D worm-like aggregates can form in solution (**Figure 1b**). Appropriate further growth (**Figure 1c**) of conjugated polymers from worm-like assemblies could lead to network-like assemblies in solution (**Figure 1d**). Finally, 2D monolayer networks can be deposited on substrates without size limitation and with high uniformity (**Figure 1e**).

To obtain conjugated polymer films from solution, dip-coating, a scalable film fabrication method, was adopted.^[28,29] Benzodifurandione-based oligo(*p*-phenylene vinylene) (BDOPV), a typical n-type building block^[30,31] was used to demonstrate the application of our monolayer deposition method (**Figure 2a**). Since solvent and solution concentration is important to the multi-level self-assembly process, we tune

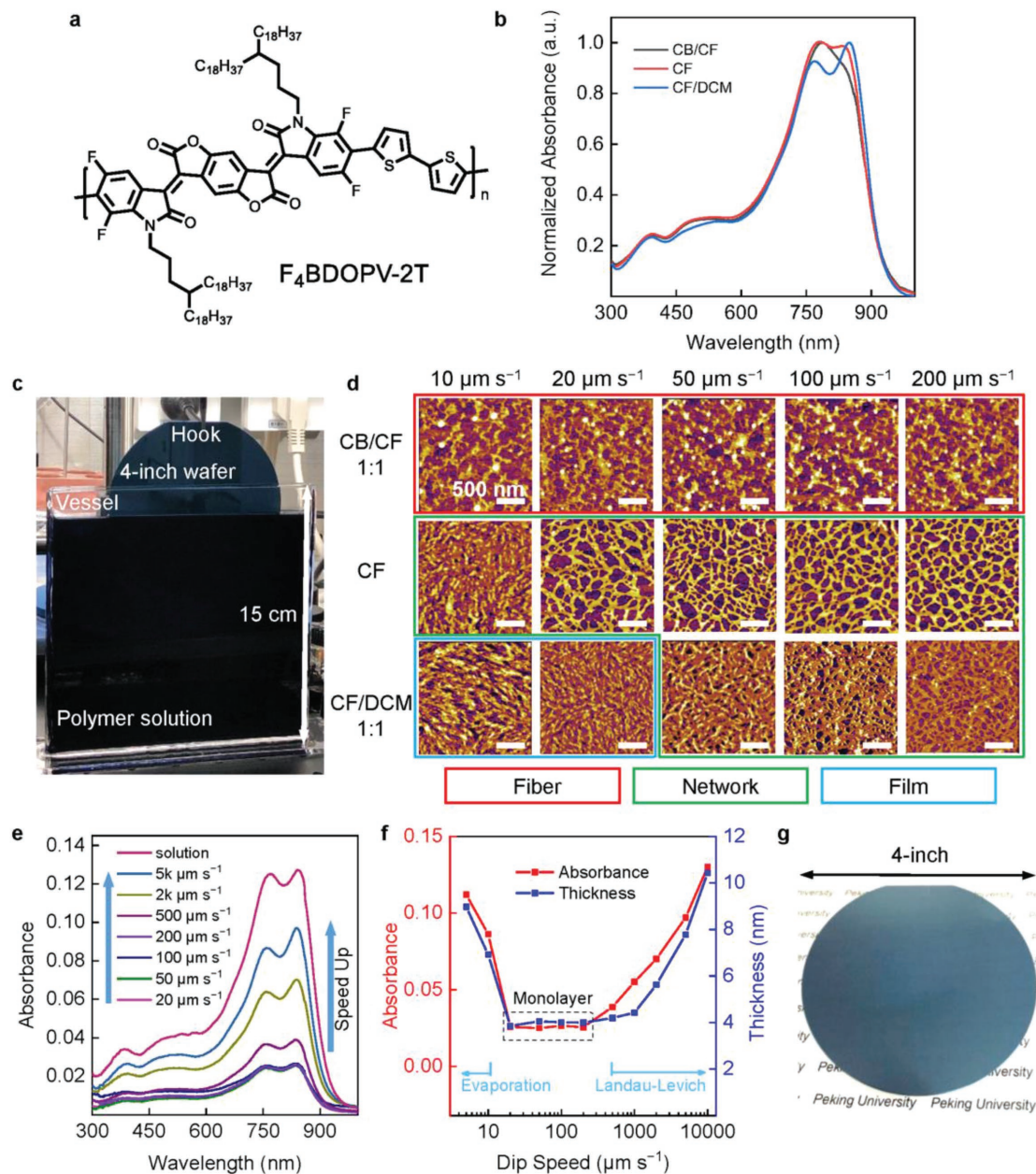


Figure 2. Wafer-scale 2D monolayer networks of conjugated polymers. a) Molecular structures of $F_4BDOPV-2T$. b) Absorption spectroscopy of $F_4BDOPV-2T$ in mixed solutions (CB: chlorobenzene, CF: chloroform, DCM: dichloromethane). c) Optical image of homemade dip-coating equipment in air for depositing wafer-scale films. d) AFM height images of films deposited on SiO_2/Si substrates at different dip-coating speed from 1 $mg mL^{-1}$ solution (50% CB + 50% CF, 100% CF, and 50% CF + 50% DCM). e) Absorption spectroscopy of $F_4BDOPV-2T$ in dilute solution (0.005 $mg mL^{-1}$ chloroform solution) and as thin films. Polymer films were deposited on borosilicate glass substrates by dip-coating from 1 $mg mL^{-1}$ chloroform solution at different dip-coating speeds. f) Absorbance at 840 nm and the corresponding thickness of polymer thin films deposited at different dip-coating speeds. The range to form monolayer polymer films is circled within the dash-line frame. g) Optical image of 4 in. wafer-scale monolayer network of $F_4BDOPV-2T$ on SiO_2/Si substrate.

the self-assembly process by different types of solvent and varying the solution concentrations. From the absorption spectra (Figure 2b), we found that relative to chloroform, dichloromethane is a poor solvent, whereas chlorobenzene is a good solvent. In good (or poor) solvent, interactions between polymers and solvents (or interactions between polymer chains) are energetically favorable and will cause expanded

(or contracted) polymer coils.^[32] When dichloromethane, a poor solvent, was added into the solution, the absorption spectra evolved in the same way as decreasing of temperature (Figure S1, Supporting Information). In contrary, adding chlorobenzene, a good solvent, the absorption spectra evolved as increasing the temperature (Figure S1, Supporting Information). These results suggest that the solution-state

assemblies can be easily controlled by mixing different types of solvent, enabling the tuning of the multi-level assemblies of conjugated polymers in the solution state.

A homemade dip-coating equipment (Figure 2c and Figure S2, Supporting Information) was used under ambient conditions with a relative humidity of 20–50%. The atomic force microscope (AFM) height images of the deposited films display the morphology evolution against solvent (Figure 2d and Table S1, Supporting Information). For dichloromethane and chloroform mixed solution, monolayer networks only appeared in a relatively smaller speed window from 50 to 500 $\mu\text{m s}^{-1}$, while films became thicker when speeds were lower than 50 $\mu\text{m s}^{-1}$ or higher than 500 $\mu\text{m s}^{-1}$. Because of the strong dispersing ability of chlorobenzene toward conjugated polymer, discrete polymer fibers and noncontinuous films were obtained under different dip-coating speed from the mixture of chlorobenzene and chloroform. After tuning the solvent and dip-coating speed, from the chloroform solution, 2D monolayer networks with uniform morphologies were obtained within a large speed window of 20 to 500 $\mu\text{m s}^{-1}$ (Figure 2d and Figure S3, Supporting Information), which ensure good experimental condition endurance for obtaining uniform monolayer networks. We note that the good connections across the network fibers might benefit the charge transport. Finally, optimized experimental condition for F₄BDOPV-2T to obtain monolayer film was using 1 mg mL⁻¹ chloroform solution at room temperature.

For monolayer from the chloroform solution, the similar area occupied percentage of about 50% was obtained at the dip-coating speed between 20 and 200 $\mu\text{m s}^{-1}$ and increased to 75% as dip-coating speed increased to 500 $\mu\text{m s}^{-1}$. Film thickness increased with decreasing speed under 20 $\mu\text{m s}^{-1}$, under which condition, the film formation was controlled by solvent evaporation. As dip-coating speed increased from 20 to 200 $\mu\text{m s}^{-1}$, the polymer monolayers were achieved. The thickness of monolayer is about 3.5 to 4.5 nm as estimated from AFM height images (Figure S3, Supporting Information). The average width of the network fibers in the monolayer is about 70 to 90 nm (Figure S4, Supporting Information). Histograms of network pore widths provided the uniform pore size with diameters of around 150 nm (Figure S5, Supporting Information). Films deposited at 500 $\mu\text{m s}^{-1}$ have higher area-occupied-ratio, yet smaller fiber width and pore size in the networks. With dip-coating speed increasing to over 500 $\mu\text{m s}^{-1}$ (from 1 to 10 k $\mu\text{m s}^{-1}$ in our experiment condition), due to liquid drag-out force, continuous multilayer films were obtained (called Landau–Levich region).^[13,33] This effect of pull speed in dip-coating on the film thickness and morphology is summarized in Figure S6 and Table S2 in the Supporting Information. Absorption spectroscopy experiments (Figure 2e) were performed to verify the film thickness due to the high sensitivity to polymer layers. The absorbance exhibits good coincidence of AFM height of polymer films under different dip-coating speeds (Figure 2f).

Solution process, such as shearing and blade coating methods, uniformity is limited by the edge effect, coffee ring effect, and thickness variation.^[29,34,35] Wide fabrication condition window is important to obtain the uniform and large-scale electronics because small condition variations will not significantly affect the film morphology. Polymer self-assembly

assistant dip-coating process in our work has a large dip-coating speed window to obtain uniform 2D monolayer conjugated polymer network. Highly uniform wafer-scale monolayer networks (Figure 2g) were fabricated directly at 100 $\mu\text{m s}^{-1}$ under optimized condition. Excellent uniformity of morphologies and microstructures on the 4 in. wafer was confirmed by AFM measurement (Figure S7, Supporting Information). Monolayer on 100 cm² quartz shows a high transparency of >93% between 300 and 1000 nm (Figure S8, Supporting Information). This method allows us to achieve large-scale and uniform polymer monolayers for scalable fabrication of polymer electronics.

Except for SiO₂/Si, other often used substrates, including inorganic (Si, SiO₂, and borosilicate glass, gold) and organic (divinyltetramethyldisiloxane-bis(benzocyclobutene) (BCB), a cross-linked polymer), and self-assembled monolayer (SAM) modified SiO₂ were used for the polymer monolayer deposition. Similar monolayer networks were observed on all of these substrates with different surface properties. These substrates covered contact angles in the range of 29–103°. (Figures S9 and S10, Supporting Information). We note that the polymer films are difficult to be deposited on the octadecyltrichlorosilane (ODTS) modified SiO₂ substrate due to its high surface energy and large contact angle of 105°. The substrate insensitivity with various surface properties suggests that strong polymer inter-chain aggregation in solution might play a critical role during deposition.^[36] After polymer films coating, the contact angle increased obviously for all various substrates (Figure S10, Supporting Information), in consistent with the more hydrophobic nature of alkyl chains of the polymer monolayer.

Grazing incidence wide-angle X-ray scattering (GIWAXS) experiments were performed on monolayer and multilayer films deposited from different dip-coating speeds (Figure 3a,b and Figure S11, Supporting Information). From 2D pattern and 1D GIWAXS plots, obvious (100), (200), (300), and (400) diffraction peaks were obtained along the out-of-plane direction. Similar diffraction patterns remain from all the thin films with different number of layers, indicating that edge-on packing mode is adopted both in the dip-coated monolayers and multilayers. As the polymer thickness decreases, the intensity of the diffraction peaks decreases obviously. For monolayer films, only weak (100) and (200) diffraction peaks can be observed. The higher order scattering peaks might result from the periodicity of electron density in the out-of-plane direction due to the structure of conjugated bones with two side alkyl chains. Electron density map reconstructed from the diffraction peaks in GIWAXS (Table S3, Supporting Information) agreed well with edge-on molecular packing mode of polymer chains (Figure 3c,d).^[37]

To characterize the charge transport properties of the 2D monolayer network, we fabricated TFT devices of F₄BDOPV-2T with a bottom-gate/top-contact (BG/TC) configuration. 4 in. wafer-scale polymer networks were deposited on BCB modified SiO₂/Si substrates at 100 $\mu\text{m s}^{-1}$ in air. Then 35 nm Au was thermal-evaporated on films as the source and drain electrodes (Figure 4a and Figure S12a, Supporting Information). Monolayer networks of F₄BDOPV-2T exhibited typical n-type carrier transport properties (Figure 4b,c) with excellent air stability. The device showed very stable gate-biased on or off current for 1500 s under the air atmosphere (Figure 4d). Output

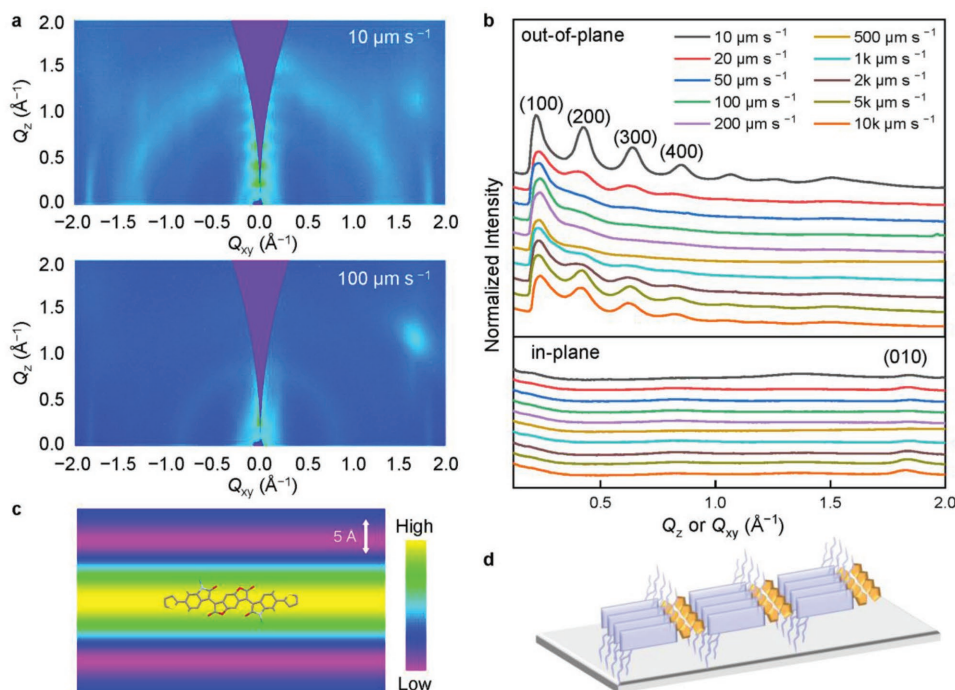


Figure 3. Molecular packing modes in thin-films. a) Representative 2D GIWAXS images of the polymer film from 10 and 100 $\mu\text{m s}^{-1}$, show clear (h00) diffraction peaks along the out-of-plane direction. b) 1D GIWAXS plots along out-of-plane and in-plane directions. c) Reconstructed vertical electron density map of the polymer monolayer. d) Schematic illustration of the edge-on polymer packing mode.

characteristics (Figure 4c) showed near-ideal characteristics and no obvious injection barrier were observed, suggesting negligible contact resistance between the polymer and electrode. Polymer monolayer transistors exhibited the highest electron mobility of $1.88 \text{ cm}^2 \text{ V}^{-1} \text{ s}^{-1}$ with the average value of $1.17 \text{ cm}^2 \text{ V}^{-1} \text{ s}^{-1}$, fabricated and measured under ambient conditions (Figure 4e). We also fabricated the transistors on bare SiO_2/Si substrates, which showed electron mobility of $0.17 \pm 0.07 \text{ cm}^2 \text{ V}^{-1} \text{ s}^{-1}$ (Figure S13, Supporting Information). Compared with BCB modified SiO_2/Si substrate, the performance decrease using bare SiO_2/Si substrate might be due to the charge trapping effects of the hydroxyl groups on SiO_2 surface.^[38,39] The dip-coating polymer monolayer films showed comparable or even higher electron mobilities compared with those fabricated by spin-coating method (Figure 4e). All the $\text{F}_4\text{BDOPV-2T}$ monolayer-based TFTs showed excellent on/off current ratio of $>10^5$ with small hysteresis, implying few electron traps in monolayer network even under ambient conditions. We tested 60 TFTs on the 4 in. wafer, and all the positions exhibited uniform electron mobilities among $0.89 \pm 0.36 \text{ cm}^2 \text{ V}^{-1} \text{ s}^{-1}$ (Figure 4f and Figure S12b, Supporting Information). TFTs based on $\text{F}_4\text{BDOPV-2T}$ monolayers exhibited high uniformity on the 4 in. wafer and excellent device performance, to our knowledge, which is the highest electron mobilities among polymer monolayer transistors (Figure 4g).^[8–10]

In the 2D monolayer TFT of $\text{F}_4\text{BDOPV-2T}$, the carrier mobility diminished with reducing temperature, indicating a thermal-activated hopping mechanism (Figure S14, Supporting Information). The activation energy (E_a) was calculated to be 96 meV using Arrhenius equation: $\mu = A \exp(-E_a/k_B T)$, where μ is the charge carrier mobility, T is the temperature, k_B is the

Boltzmann constant, and A is the pre-exponential factor.^[40] Contact resistance (Figure 4h) of TFT devices based on dip-coated monolayer (4 nm) and spin-coated multilayer (18 nm) as a control group was measured via the modified transmission-line method (M-TLM).^[41] TFT devices of the dip-coated monolayer networks showed almost one order of magnitude lower contact resistance, compared with that of the spin-coated film (Figure 4i). Lower contact resistance can be largely explained by the thinner injection pathways and the porosity of the monolayer film.^[42]

To evaluate the polymer monolayer and gold electrodes interface properties, we quantitatively analyzed the Schottky barrier height (SBH) of our TFTs. The source–drain current (I_{DS}) at the subthreshold region mainly depends on the thermionic emission and the thermally assisted tunneling. According to this theory, the channel current (I_{DS}) can be written as a function of temperature (T)^[42,43]: $I_{\text{DS}} = AA^* T^{3/2} \exp(-q\Phi_B/k_B T)$, where A is contact area, A^* is the 2D effective Richardson constant, q is the electronic charge, Φ_B is the Schottky barrier height, and k_B is the Boltzmann constant. Below flat-band voltage (V_{FB}), thermionic emission mechanism dominates the channel current, leading to a linear dependence of Φ_B versus gate voltage (V_G). When V_G is larger than V_{FB} , thermally assisted tunneling current becomes significant, which results in the nonlinear behavior. The SBH for a given gate voltage can be estimated from the slope of the plot of $\ln(I_{\text{DS}}/T^{3/2})$ against $1000/T$ (Figure 4j). The true SBH is 415 meV for dip-coated monolayer and 1.12 eV for spin-coated multilayer which were determined according to the linear dependence of Φ_B on V_G (Figure 4k). The polymer monolayer shows lower SBH and less contact resistance, which can benefit for short channel and high-speed circuits.

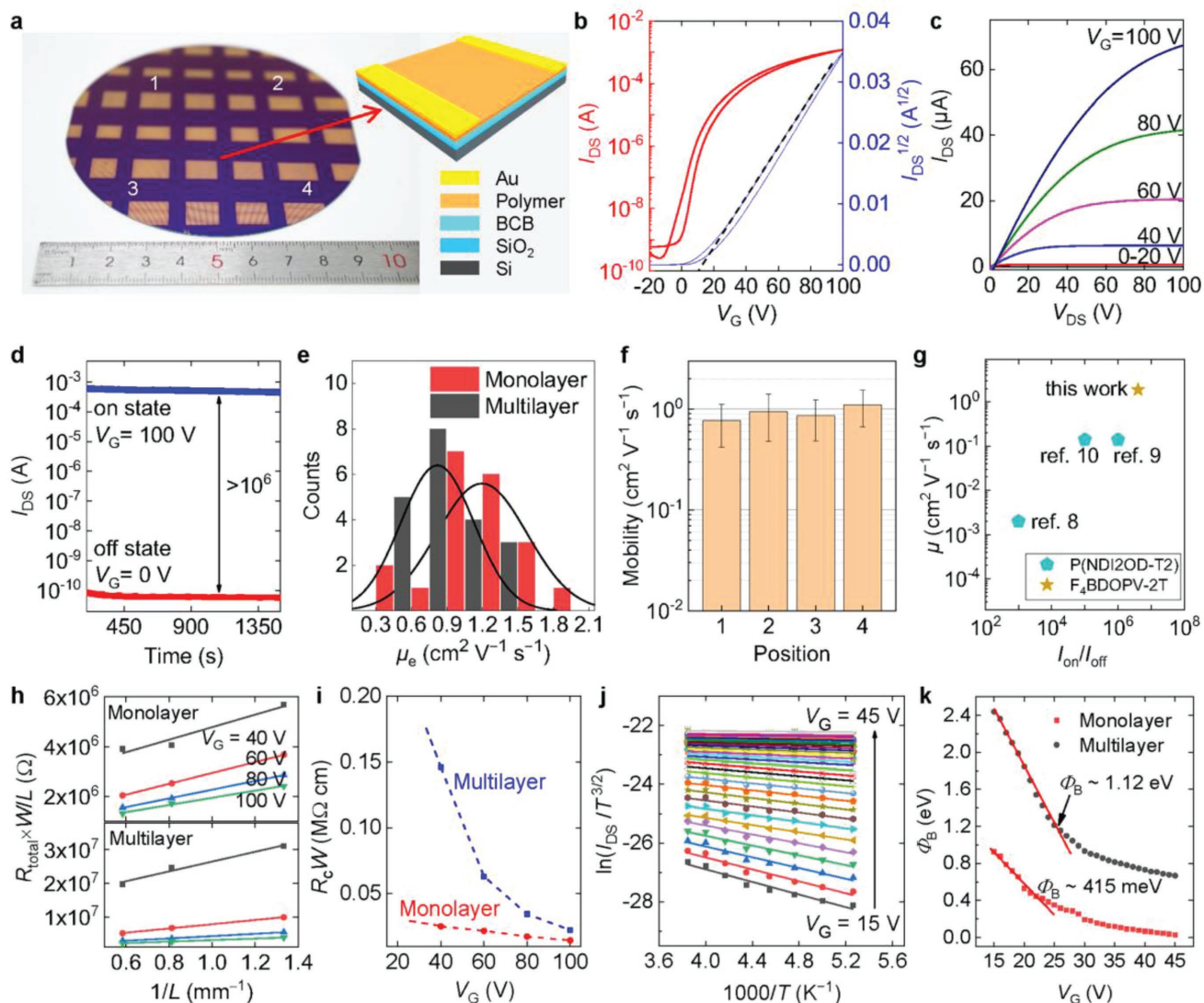


Figure 4. TFT devices and charge transport performance. a) TFT devices fabricated on a 4 in. wafer using top-contact/bottom-gate configuration. b) Representative transfer characteristics and c) output characteristics of a TFT device based on the 2D monolayer network of F₄BDOPV-2T. d) Gate voltage bias stability of a monolayer TFT, showing excellent bias stability with high on/off ratios >10⁶ after biasing over 1500 s. e) Histograms and distributions of the electron mobilities extracted from the polymer monolayer TFT devices and the spin-coated multilayer TFT devices. f) Histogram of mobilities measured on different positions on a 4 in. wafer a), which showed excellent uniformity on a whole wafer. g) Electron mobility and on/off current ratio comparison of our polymer monolayer TFT devices and other n-type polymer monolayers. h) Contact resistance measurement via the modified transmission-line method of spin-coated multilayer (18 nm) and dip-coated monolayer (4 nm). i) Comparison of contact resistance under different gate voltage of spin-coated and dip-coated thin film TFTs. j) Arrhenius plot of $\ln(I_{DS}/T^{3/2})$ of monolayer TFT under different gate voltages. k) Extracted Schottky barrier heights obtained from Arrhenius fit of $\ln(I_{DS}/T^{3/2})$ of TFTs for the dip-coated monolayer and spin-coated multilayer devices.

The absorption spectroscopy of polymer films is almost the same as those of dilute chloroform solutions (Figure 2e), implying that the aggregates had already formed in solution. To further investigate the monolayer formation mechanism, we combine solution absorption spectroscopy, small angle neutron scattering (SANS), molecular dynamics (MD) simulation, and freeze-drying method to understand the assemblies' structures and further growth of conjugated polymer from solution-state to solid-state.

For SANS experiments, deuterated solvents were used, because of the distinct scattering length densities (SLDs) between polymers and deuterated solvents.^[44] For a high

signal-to-noise ratio, a solution of F₄BDOPV-2T in deuterated chloroform (3 mg mL⁻¹) was used for scattering experiments (Figure 5a). The scattering data were fitted well to Porod plot of $I(Q) \approx Q^{-\alpha}$, where α (Porod exponent) is the fractal dimension of the scattering objects in solution.^[44] The fitted Porod exponent is 1.10, indicated 1D rod-like aggregates were formed in solution (Figure S15, Supporting Information). Worm-like chain model (Figure 5a,b), which describes the semirigid chains, fits best with the experimental data.^[45] Three critical parameters describing the dimensions of worm-like chain (Figure 5b) are contour length (L_{chain} , 132 nm) of the semirigid chain, the Kuhn length (69.1 nm) of a rigid repeating unit (equals to $2L_p$,

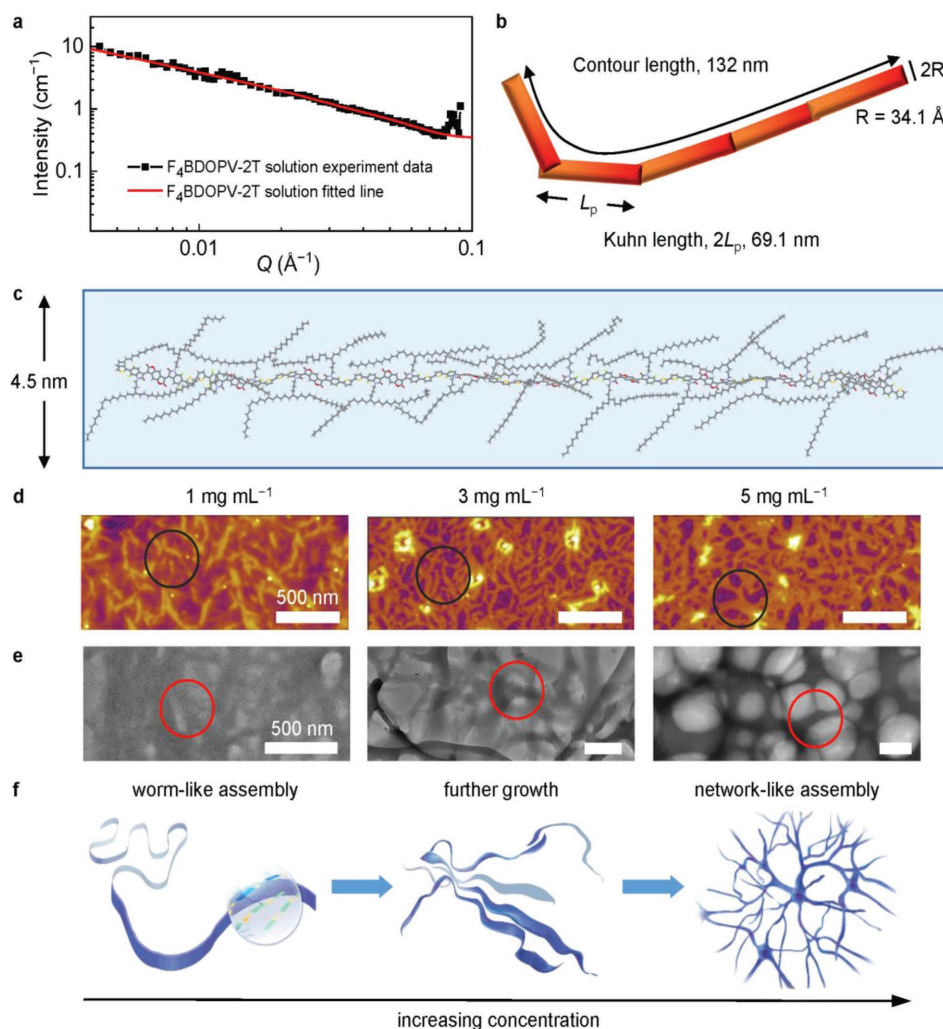


Figure 5. Multi-level self-assemblies of conjugated polymers. a) SANS intensity curve of 3 mg mL⁻¹ chloroform solution of F₄BDOPV-2T. b) 1D worm-like chain model of F₄BDOPV-2T in chloroform solution inferred from SANS data. c) The simulated molecular conformation of a single polymer chain with 10 repeating units. Hydrogen atoms are omitted for clarity. d) AFM height images and e) TEM images of F₄BDOPV-2T assemblies obtained by freeze-drying from chloroform solutions with different concentration: 1, 3, and 5 mg mL⁻¹. Scale bars correspond to 500 nm in all AFM and TEM images. f) Corresponding schematic diagram of assembly development process in the concentration-gradient region.

where L_p is persistence length), and radius (R , 34.1 Å). The large L_{chain} implies that multiple polymer chains composed the 1D aggregates via strong π - π stacking interactions between the polymer backbones. Kuhn length of 69.1 nm (about 28 polymeric repeating units) shows a rigid polymer chain segment. Furthermore, the structure of F₄BDOPV-2T in solution state was constructed and optimized by combining quantum calculations (Figure S16, Supporting Information) and molecular dynamics (Figure S17, Supporting Information). The conformation of a polymer chain shows an approximately single-chain width of 4.5 nm (Figure 5c), which is coincident with the radius of the worm-like model inferred from SANS data.

Freeze-drying experiments of the polymer solution was carried out for direct observation of polymer aggregates in solution-state. It is an effective and visual approach to observe unstable solution-state supramolecular structures of conjugated polymers. The polymer solution was carefully dropped onto a silicon substrate or copper grid and then was immediately

put into a Schlenk flask in liquid nitrogen bath for freezing polymer aggregates. The solvent, chloroform was sublimated under a persistent vacuum system. The polymer solutions with the various concentrations of 1, 3, and 5 mg mL⁻¹ were freeze-dried. AFM height images (Figure 5d) and transmission electron microscope (TEM, Figure 5e) images of freeze-dried films directly demonstrate the structures of polymer aggregates in solution-state, which behaved like fibers or networks. The longitudinal lengths of polymer aggregates are in the range from 80 to 300 nm, which agreed well with the contour length from SANS data fitting. In addition, the aggregates grew up at higher concentration, forming several nodes of fibers and network-like assemblies, indicating the polymer growth in solution process within the concentration-gradient region.^[46] The microscopic images of freeze-dried films provided a distinct picture of multi-level self-assembly process along with the increasing concentration (Figure 5f). Polymeric network-like assemblies will form in high-concentration during the deposition

process, such as the meniscus in the dip-coating process. In a word, controlled multi-level self-assemblies from worm-like to network-like assemblies of polymers make their monolayer network morphology independent of the substrates. On the basis of these experimental and theoretical results, we can conclude that stronger polymer interchain interactions in solution can promote the formation of the polymer monolayer films without the size and substrate limitations.

In summary, our work demonstrates an effective approach to obtain wafer-scale and uniform polymer monolayer films, which is enabled by controlling the multi-level self-assembly process of conjugated polymers. Wafer-scale polymer monolayer transistor arrays were successfully fabricated and exhibited excellent charge transport properties with good stability in air. Polymer monolayer FETs exhibited high electron mobilities of up to $1.88 \text{ cm}^2 \text{ V}^{-1} \text{ s}^{-1}$, which is comparable or even better device performance than conventional spin-coated films but with almost one of magnitude smaller contact resistances. By probing the self-assembly process of conjugated polymers, 1D rod-like polymer aggregates were found in solution, which can further grow to 2D network-like assemblies and polymer monolayers. We found that the solution-state assemblies might be the fundamental reason for the highly uniform 2D monolayer networks. Our method provides a substrate-independent, wafer-scale, and uniform 2D monolayer film fabrication method with high transistor performances. We believe that our result can further advance the practical application of conjugated polymers for low-cost and large-scale complex electronics.

Supporting Information

Supporting Information is available from the Wiley Online Library or from the author.

Acknowledgements

This work was supported by National Key R&D Program of China (2017YFA0204701), National Natural Science Foundation of China (21420102005, 21790360, 21722201, and 91427303), and the U.S. Department of Energy, Office of Science, Office of Basic Energy Sciences under award number of SC0019361. Use of the Stanford Synchrotron Radiation Lightsource, SLAC National Accelerator Laboratory, was supported by the U.S. Department of Energy, Office of Science, Office of Basic Energy Sciences under Contract No. DE-AC02-76SF00515. The authors thank beamline BL14B1 (Shanghai Synchrotron Radiation Facility) for providing the beam time.

Conflict of Interest

The authors declare no conflict of interest.

Keywords

2D organic materials, conjugated polymers, multi-level assemblies, polymer monolayers

Received: October 17, 2018

Revised: November 30, 2018

Published online: December 14, 2018

- [1] C. Tan, X. Cao, X.-J. Wu, Q. He, J. Yang, X. Zhang, J. Chen, W. Zhao, S. Han, G.-H. Nam, M. Sindoro, H. Zhang, *Chem. Rev.* **2017**, *117*, 6225.
- [2] K. S. Novoselov, A. Mishchenko, A. Carvalho, A. H. Castro Neto, *Science* **2016**, *353*, aac9439.
- [3] F. Yang, S. Cheng, X. Zhang, X. Ren, R. Li, H. Dong, W. Hu, *Adv. Mater.* **2018**, *30*, 1702415.
- [4] K. S. Novoselov, A. K. Geim, S. V. Morozov, Y. Z. D. Jiang, S. V. Dubonos, I. V. Grigorieva, A. A. Firsov, *Science* **2004**, *306*, 666.
- [5] Y. Zhang, Y.-W. Tan, H. L. Stormer, P. Kim, *Nature* **2005**, *438*, 201.
- [6] M. V. Gustafsson, M. Yankowitz, C. Forsythe, D. Rhodes, K. Watanabe, T. Taniguchi, J. Hone, X. Zhu, C. R. Dean, *Nat. Mater.* **2018**, *17*, 411.
- [7] M. Li, D. K. Mangalore, J. Zhao, J. H. Carpenter, H. Yan, H. Ade, H. Yan, K. Müllen, P. W. M. Blom, W. Pisula, D. M. de Leeuw, K. Asadi, *Nat. Commun.* **2018**, *9*, 451.
- [8] S. Fabiano, C. Musumeci, Z. Chen, A. Scandurra, H. Wang, Y.-L. Loo, A. Facchetti, B. Pignataro, *Adv. Mater.* **2012**, *24*, 951.
- [9] D. Khim, G.-S. Ryu, W.-T. Park, H. Kim, M. Lee, Y.-Y. Noh, *Adv. Mater.* **2016**, *28*, 2752.
- [10] S. G. Bucella, A. Luzio, E. Gann, L. Thomsen, C. R. McNeill, G. Pace, A. Perinot, Z. Chen, A. Facchetti, M. Caironi, *Nat. Commun.* **2015**, *6*, 8394.
- [11] D. He, J. Qiao, L. Zhang, J. Wang, T. Lan, J. Qian, Y. Li, Y. Shi, Y. Chai, W. Lan, L. K. Ono, Y. Qi, J.-B. Xu, W. Ji, X. Wang, *Sci. Adv.* **2017**, *3*, e1701186.
- [12] Y. Shi, L. Jiang, J. Liu, Z. Tu, Y. Hu, Q. Wu, Y. Yi, E. Gann, C. R. McNeill, H. Li, W. Hu, D. Zhu, H. Sirringhaus, *Nat. Commun.* **2018**, *9*, 2933.
- [13] L. Li, P. Gao, W. Wang, K. Müllen, H. Fuchs, L. Chi, *Angew. Chem., Int. Ed.* **2013**, *52*, 12530.
- [14] S. Arai, S. Inoue, T. Hamai, R. Kumai, T. Hasegawa, *Adv. Mater.* **2018**, *30*, 1707256.
- [15] T. Yokota, T. Kajitani, R. Shidachi, T. Tokuhara, M. Kaltenbrunner, Y. Shoji, F. Ishiwari, T. Sekitani, T. Fukushima, T. Someya, *Nat. Nanotechnol.* **2018**, *13*, 139.
- [16] P. Lin, F. Yan, *Adv. Mater.* **2012**, *24*, 34.
- [17] C. Sutton, C. Risko, J.-L. Brédas, *Chem. Mater.* **2016**, *28*, 3.
- [18] S. K. Park, J. H. Kim, S. Y. Park, *Adv. Mater.* **2018**, *30*, 1704759.
- [19] A. Yamamura, S. Watanabe, M. Uno, M. Mitani, C. Mitsui, J. Tsurumi, N. Isahaya, Y. Kanaoka, T. Okamoto, J. Takeya, *Sci. Adv.* **2018**, *4*, eaao5758.
- [20] Y. Jiang, J. Chen, Y. Sun, Q. Li, Z. Cai, J. Li, Y. Guo, W. Hu, Y. Liu, *Adv. Mater.* **2018**, *1805761*, <https://onlinelibrary.wiley.com/doi/full/10.1002/adma.201805761>.
- [21] Q. Wang, F. Yang, Y. Zhang, M. Chen, X. Zhang, S. Lei, R. Li, W. Hu, *J. Am. Chem. Soc.* **2018**, *140*, 5339.
- [22] H. Yan, Z. Chen, Y. Zheng, C. Newman, J. R. Quinn, F. Dötz, M. Kastler, A. Facchetti, *Nature* **2009**, *457*, 679.
- [23] H. Minemawari, T. Yamada, H. Matsui, J. Tsutsumi, S. Haas, R. Chiba, R. Kumai, T. Hasegawa, *Nature* **2011**, *475*, 364.
- [24] V. D'Innocenzo, A. Luzio, H. Abdalla, S. Fabiano, M. A. Loi, D. Natali, A. Petrozza, M. Kemerink, M. Caironi, *J. Mater. Chem. C* **2016**, *4*, 11135.
- [25] M. A. C. Stuart, W. T. S. Huck, J. Genzer, M. Müller, C. Ober, M. Stamm, G. B. Sukhorukov, I. Szleifer, V. V. Tsukruk, M. Urban, F. Winnik, S. Zauscher, I. Luzinov, S. Minko, *Nat. Mater.* **2010**, *9*, 101.
- [26] B. B. Patel, Y. Diao, *Nanotechnology* **2018**, *29*, 0444004.
- [27] Y.-Q. Zheng, Z.-F. Yao, T. Lei, J.-H. Dou, C.-Y. Yang, L. Zou, X. Meng, W. Ma, J.-Y. Wang, J. Pei, *Adv. Mater.* **2017**, *29*, 1701072.
- [28] J. Jang, S. Nam, K. Im, J. Hur, S. N. Cha, J. Kim, H. B. Son, H. Suh, M. A. Loth, J. E. Anthony, J. J. Park, C. E. Park, J. M. Kim, K. Kim, *Adv. Funct. Mater.* **2012**, *22*, 1005.
- [29] S. K. Garlapati, M. Divya, B. Breitung, R. Kruk, H. Hahn, S. Dasgupta, *Adv. Mater.* **2018**, *30*, 1707600.

- [30] T. Lei, J.-H. Dou, X.-Y. Cao, J.-Y. Wang, J. Pei, *J. Am. Chem. Soc.* **2013**, *135*, 12168.
- [31] Y.-Q. Zheng, T. Lei, J.-H. Dou, X. Xia, J.-Y. Wang, C.-J. Liu, J. Pei, *Adv. Mater.* **2016**, *28*, 7213.
- [32] F. Brochard, P. G. de Gennes, *Macromolecules* **1977**, *10*, 1157.
- [33] M. Le Berre, Y. Chen, D. Baigl, *Langmuir* **2009**, *25*, 2554.
- [34] A. C. Arias, J. D. MacKenzie, I. McCulloch, J. Rivnay, A. Salleo, *Chem. Rev.* **2010**, *110*, 3.
- [35] K. Fukuda, T. Someya, *Adv. Mater.* **2017**, *29*, 1602736.
- [36] N. Chiang, N. Jiang, L. R. Madison, E. A. Pozzi, M. R. Wasielewski, M. A. Ratner, M. C. Hersam, T. Seideman, G. C. Schatz, R. P. Van Duyne, *J. Am. Chem. Soc.* **2017**, *139*, 18664.
- [37] B. Chen, X. Zeng, U. Baumeister, G. Ungar, C. Tschierske, *Science* **2005**, *307*, 96.
- [38] L.-L. Chua, J. Zaumseil, J.-F. Chang, E. C.-W. Ou, P. K.-H. Ho, H. Sirringhaus, R. H. Friend, *Nature* **2005**, *434*, 194.
- [39] B. Park, I. In, P. Gopalan, P. G. Evans, S. King, P. F. Lyman, *Appl. Phys. Lett.* **2008**, *92*, 90.
- [40] H. Sirringhaus, M. Bird, N. Zhao, *Adv. Mater.* **2010**, *22*, 3893.
- [41] Y. Xu, R. Gwoziecki, I. Chartier, R. Coppard, F. Balestra, G. Ghibaudo, *Appl. Phys. Lett.* **2010**, *97*, 063302.
- [42] A. Allain, J. Kang, K. Banerjee, A. Kis, *Nat. Mater.* **2015**, *14*, 1195.
- [43] H. Yang, J. Heo, S. Park, H. J. Song, D. H. Seo, K.-E. Byun, P. Kim, I. K. Yoo, H.-J. Chung, K. Kim, *Science* **2012**, *336*, 1140.
- [44] B. Hammouda, *Polym. Rev.* **2010**, *50*, 14.
- [45] I. Teraoka, *Polymer Solutions*, John Wiley & Sons, Inc., New York, USA, **2002**.
- [46] X. Gu, L. Shaw, K. Gu, M. F. Toney, Z. Bao, *Nat. Commun.* **2018**, *9*, 534.